I. J. Trans. Phenomena, Vol. 13, pp. 143–150
Reprints available directly from the publisher
Photocopying permitted by license only

Resolving the Vibrational and Electronic Contributions to Thermal Conductivity of Silicon Near the Solid-Liquid Transition: Molecular Dynamics Study

CHRISTOPHER H. BAKER[1]*, CHENGPING WU[2], RICHARD N. SALAWAY[1], LEONID V. ZHIGILEI[2] AND PAMELA M. NORRIS[1]

[1]*Department of Mechanical and Aerospace Engineering University of Virginia, 122 Engineer's Way, Charlottesville, VA 22904-4746, USA*
[2]*Department of Materials Science and Engineering University of Virginia, 395 McCormick Road, Charlottesville, VA 22904-4745, USA*

Although thermal transport in silicon is dominated by phonons in the solid state, electrons also participate as the system approaches, and exceeds, its melting point. Thus, the contribution from both phonons and electrons must be considered in any model for the thermal conductivity of silicon near the melting point. In this work, the phononic contribution to the bulk thermal conductivity of silicon is determined for the Stillinger-Weber potential in equilibrium and non-equilibrium molecular dynamics simulations for temperatures ranging from 1400 K to 2000 K. It is found that, although the contribution of electron-hole pair diffusion to high temperature conductivity of solid silicon is not included in classical molecular dynamics simulations, the Stillinger-Weber potential overestimates the vibrational contribution to thermal conductivity and, incidentally, reproduces quite well the total thermal conductivity of the solid phase up to the melting temperature. As for the liquid phase conductivity, the Stillinger-Weber potential agrees with theoretical treatment of the phononic thermal transport and predicts a minor phononic contribution of about 3% to the total liquid phase thermal conductivity. Thus, atomistic modeling of thermal transport in liquid phase silicon must include a description of the electronic contribution, e.g., through a combination of the molecular dynamics method with the continuum treatment of the electronic thermal conductivity within the two-temperature model.

Keywords: Molecular dynamics simulation, silicon, high temperature, thermal conductivity.

*Corresponding author: chb2fd@virginia.edu

INTRODUCTION

The ability of lasers to deliver large amounts of energy to a desired target with high spatial and temporal resolution is leveraged in the rapid processing of semiconductor materials where short pulse laser irradiation provides fine control in such processes as laser cutting, welding, and annealing (Bass, 1983; Migliore, 1996; Miller & Haglund, 1998; Poate & Mayer, 1982). Understanding the thermal response of silicon to laser irradiation is increasingly critical as the design requirements of modern technology continue to challenge current thermal processing of silicon and other materials.

The sensitivity to input parameters of the laser processing techniques coupled with the advancement of nanostructured, silicon-based materials necessitates an understanding of silicon's thermal behavior at the nanoscale. The molecular dynamics (MD) method is a popular technique for computational investigation of the nanoscale behavior of materials. Past MD studies of silicon have focused on its structural and thermodynamic properties in the solid and liquid states (Broughton & Li, 1987; Lee, Biswas, Soukoulis, Wang, Chan, & Ho, 1991; Stich, Car, & Parrinello, 1991). More recently, MD studies have been conducted on silicon's solid phase thermal conductivity with attention to simulation domain size effects (Hu, Evans, & Keblinski, 2011; Schelling, Phillpot, & Keblinski, 2002; Sellan, Landry, Turney, McGaughey, & Amon, 2010; Volz & Chen, 2000).

The present work focuses on modeling of silicon at temperatures near and above the melting point, as would be encountered in the laser processing of materials. In this regime, experiments have shown that electron-hole pair diffusion contributes as much as 40% to the thermal conductivity in the high temperature solid phase and free electrons dominate the liquid phase conductivity (Fulkerson, Moore, Williams, Graves, & McElroy, 1968; Glassbrenner & Slack, 1964; Yamasue, Susa, Fukuyama, & Nagata, 2002). Traditional MD simulations do not explicitly account for the electronic thermal transport, although the electronic contribution to the thermal conductivity can be accounted for in a hybrid atomistic-continuum model where MD is coupled with the two temperature model (TTM) and the electron heat diffusion equation is solved numerically on a grid that overlaps with the MD system (Duffy & Rutherford, 2007; Head-Gordon & Tully, 1995; Ivanov & Zhigilei, 2003; Phillips, Magyar, & Crozier, 2010; Rutherford & Duffy, 2007; Schall, Padgett, & Brenner, 2005). This requires information on the individual contributions of the phonons and electrons to the total thermal conductivity within the TTM-MD framework. In this work, the phononic contribution to the thermal conductivity of the model silicon material is evaluated in MD simulations performed with the Stillinger-Weber interatomic potential (Stillinger & Weber, 1985; Stillinger & Weber, 1986) in a temperature range from 1400 K to 2000 K. The electronic contribution missing in the MD model is then obtained by subtracting the results of MD simulations from the experimental values of thermal conductivity (Salaway, Hopkins, Norris, & Stevens, 2008).

METHODS

In the MD simulation method, atoms are treated as classical particles that interact via an interatomic potential. The system is then evolved according to Newton's equations of motion. In comparison to analytical techniques, MD makes no assumptions concerning phonon transport after the interatomic potential is defined. Thus, MD includes all anharmonic effects, a feature especially important for high temperature systems where larger atomic displacements lead to more anharmonicity. The Stillinger-Weber interatomic potential (Stillinger & Weber, 1985; Stillinger & Weber, 1986) is selected for this study because its original formulation used properties near the melting point as the fitting criteria, it is one of the best silicon potentials for modeling thermal effects (Schelling, Phillpot, & Keblinski, 2002), and it is prevalent in the literature.

This study uses both equilibrium molecular dynamics (EMD) and non-equilibrium molecular dynamics (NEMD) techniques to calculate the thermal conductivity of high temperature Stillinger-Weber silicon. The EMD method has been shown to return the bulk thermal conductivity of silicon even when using small system sizes (Schelling, Phillpot, & Keblinski, 2002; Sellan, Landry, Turney, McGaughey, & Amon, 2010; Volz & Chen, 2000). In this method, the fluctuation-dissipation theorem is invoked to determine the conductivity according to the Green-Kubo formalism (McQuarrie, 2000):

$$k_{\mu\nu}(\tau_f) = \frac{1}{Vk_B T^2}\int_0^{\tau_f} \langle S_\mu(\tau) S_\nu(0)\rangle d\tau, \qquad (1)$$

where $k_{\mu\nu}$ is the thermal conductivity tensor, V is the system volume, k_B is the Boltzmann constant, T is the temperature, S_μ and S_ν are the μth and νth component of the heat current $\vec{S}$, and τ is the correlation time. Theoretically, the upper integration limit of Eq. 1 is infinity, but in practice, the integration is limited by a finite correlation time, τ_f. The heat current is a measure of the thermal energy transport in the system and differs from the heat flux by a volume factor. Both the heat current and the heat flux are calculated by summing the convective and conductive contributions of each atom to the thermal transport (Schelling, Phillpot, & Keblinski, 2002):

$$\vec{S} = \sum_i \varepsilon_i \vec{v}_i + \frac{1}{2}\sum_{ij} \vec{r}_{ij}(\vec{F}_{ij}\cdot\vec{v}_i) + \frac{1}{6}\sum_{ijk}(\vec{r}_{ij}+\vec{r}_{ik})(\vec{F}_{ijk}\cdot\vec{v}_i), \tag{2}$$

where i, j, and k index different atoms, ε_i and $\vec{v}_i$ are the energy and velocity of atom i, $\vec{r}_{ij}$ is the distance between atoms i and j, $\vec{F}_{ij}$ is the two body force acting on atom i due to neighbor j, and $\vec{F}_{ijk}$ is the three body force term acting on atom i. This is a general formulation for an interatomic potential represented by contributions from two- and three-body interactions. The forces can be calculated from the Stillinger-Weber potential (Stillinger & Weber, 1985; Stillinger & Weber, 1986).*

The term appearing in brackets in Eq. 1 is the heat current autocorrelation function (HCACF), given by:

$$\langle S_\mu(\tau)S_\nu(0)\rangle = \frac{1}{t_f-\tau}\int_0^{t_f-\tau} S_\mu(t+\tau)S_\nu(t)dt, \tag{3}$$

where t is simulation time. In practice, the integrals in Eqs. 1 and 3 become summations due to the discrete nature of simulations.

In essence, the Green-Kubo formalism uses the decay time of fluxes resulting from instantaneous temperature gradients to determine the thermal conductivity. The advantages of this technique are that the full thermal conductivity tensor can be obtained from one simulation and fewer than 10,000 atoms are needed to model the bulk thermal transport (Sellan, Landry, Turney, McGaughey, & Amon, 2010), reducing the computational workload compared to NEMD. One drawback of the method, as evidenced in Results and Discussion, is that the results can be difficult to interpret due to random fluctuations of the HCACF. The impact of the fluctuations on the analysis can be mitigated by conducting multiple simulations and averaging. The results of EMD studies can be further validated by NEMD studies, which allow for an easier interpretation of the results but require larger simulation systems.

Non-equilibrium molecular dynamics uses Fourier's law,

$$\vec{q} = -k\nabla T \tag{4}$$

to calculate the thermal conductivity, k, where $\vec{q}$ and ∇T are the applied flux and temperature gradient, respectively. In this method, the system is brought to a desired temperature, and then a heat flux is applied by adding kinetic energy to the hot heat bath maintained at one end of the system, and removing kinetic energy from the cold heat bath maintained at the other end. After the system equilibrates, data are collected by averaging over time and the resulting temperature profile is used to obtain k. For any finite length domain, especially for those smaller than the mean free path of the dominant heat carrying phonons, some carriers will travel ballistically from one heat bath to the other. This decreases the thermal conductivity compared to the bulk value through the premature scattering of these phonons at the bath interfaces. Nevertheless, bulk conductivity values may be estimated through the "linear extrapolation procedure" (Hu, Evans, & Keblinski, 2011; Schelling, Phillpot, & Keblinski, 2002; Sellan, Landry, Turney, McGaughey, & Amon, 2010) applied to the results of the simulations performed for different lengths of the computational domain. In the linear extrapolation procedure, the length dependent conductivity values are plotted against L^{-1} and k^{-1} axes, where L is the system length. When the smallest system length is on the order of the mean free path of the dominant heat carrying phonons (Sellan, Landry, Turney, McGaughey, & Amon, 2010) and when the aspect ratio of the system is less than approximately 200 (Hu, Evans, & Keblinski, 2011), the data fit a linear trend with respect to the inverted axes, which, when extrapolated to $L^{-1} = 0$, gives the bulk conductivity.

* Note that due to the form of the Stillinger-Weber potential, there are multiple methods of calculating the force that differ in computational speed but not the end result.

SIMULATION DETAILS

All simulations were carried out with LAMMPS (Plimpton, 1995). The thermal conductivity of silicon was calculated using EMD for temperatures between 1400 and 2000 K and using NEMD for temperatures between 1600 and 1700 K. For a perfectly homogeneous, isotopically pure, defect free system, the lack of heterogeneous nucleation sites for phase transformations allows the system to remain in the solid state up to about 25% above the melting temperature or in the liquid state below the melting temperature on the time scales of the simulations, even though these states are not thermodynamically favorable. As such, the initial temperatures were set in all simulations such that the system was solid at 1600 K and below and liquid at 1700 K and above.

For the EMD and NEMD approaches, the equilibrium density for the various temperatures was first found through a set of preliminary simulations.[†] In these simulations, a crystalline system with a lattice constant of 0.543 nm was generated. The system was then brought to the target value of temperature and a pressure of 1 bar in MD simulations performed over the course of 50 ps (solid phase) or 100 ps (liquid phase) with the Nosé-Hoover barostat and thermostat (Hoover, 1985; Nosé, 1984). The relaxation time of 1.0 ps was used in the baro/thermostats and the time step of the integration of the atomic equations of motion was 0.5 fs. For the solid phase, the initial velocity distribution corresponded to the target temperature whereas for the liquid phase, the initial velocity distribution was set to 3000 K to ensure the completely melted state. After the desired system temperature was reached, the system was equilibrated for another 50 ps, after which the equilibrium density of the material was found by averaging over 2 ns of the constant pressure, constant temperature simulation (Tab. 1). The density tends to decrease with temperature, except for the solid to liquid transition where the density increases by about 7.7%. This result agrees with the literature value of 7.6% for Stillinger-Weber silicon at zero bar of pressure (Broughton & Li, 1987). The experimental value of the density change is about 11.4% (Ohsaka, Chung, Rhim, & Holzer, 1997).

In the EMD simulations, the equilibrium density obtained in the preliminary simulations was used to generate an $8 \times 8 \times 8$ unit cell silicon crystal. The system temperature was then set using an appropriate initial velocity distribution and 50 ps (solid phase) or 100 ps (liquid phase) of simulation time with the Nosé-Hoover thermostat. The system was then equilibrated for another 50 ps, after which the thermostat was turned off. The heat current was calculated using Eq. 2 every 10 time steps for 2 ns. The HCACF was then computed with Eq. 3 for correlation times, τ, up to 800 ps, and the diagonal components averaged.

In the NEMD simulations, computational systems with dimensions of $6 \times 6 \times$ N unit cells, where N is equal to 50, 100, 150, and 200, were generated for each temperature. The systems were equilibrated using the Nosé-Hoover thermostat for 25 ps (solid) and 50 ps (liquid). The wall regions with thickness of 1 unit cell were then created and the atoms in the walls were kept rigid in the simulations. The system was further equilibrated for 50 ps. Two heat bath regions with a thickness of 3 unit cells each were then defined next to the rigid walls. The velocities of atoms within these regions were continuously rescaled to achieve a heat flux of 10 GW/m^2 (solid phase) or 2 GW/m^2 (liquid phase). After turning on the heat baths, the system was allowed to evolve to the steady state for 500 ps. The computational domain was then divided into 1 unit cell thick slices for the purpose of obtaining

TABLE 1
Equilibrium lattice constant as a function of temperature for the solid phase, or equivalent lattice constant for the liquid phase predicted in MD simulations performed under conditions of constant 1 bar of pressure. The lattice constants agree with literature values for Stillinger-Weber silicon at zero bar (Broughton & Li, 1987)

T (K)	1400	1500	1600	1700	1800	1900	2000
a (Å)	5.45605	5.45733	5.45864	5.32563	5.32963	5.33421	5.33916

[†] This allowed data to be taken in constant volume simulations, reducing oscillations in the pressure.

the spatial temperature profile and data was collected every 10 time steps for 10 ns (solid phase) or 8 ns (liquid phase). The temperature gradient was found by linearly fitting the temperature profile over the central half of the computational domain in order to avoid the non-linear effects near the heat bath regions. With the known heat flux and the temperature gradient, the conductivity was found from Eq. 4.

RESULTS AND DISCUSSION

The HCACF of the EMD simulations displays rapid reduction to zero followed by random fluctuation about zero (Fig. 1). This reduction takes place over the course of about 50 ps for the solid phase and less than 0.5 ps for the liquid phase. The shorter decay time observed for the liquid phase corresponds to a more rapid loss of correlations in atomic vibration in the highly disorganized atomic structure. One explanation for the persistent fluctuations about zero is an artificial correlation of the heat current caused by un-scattered phonon

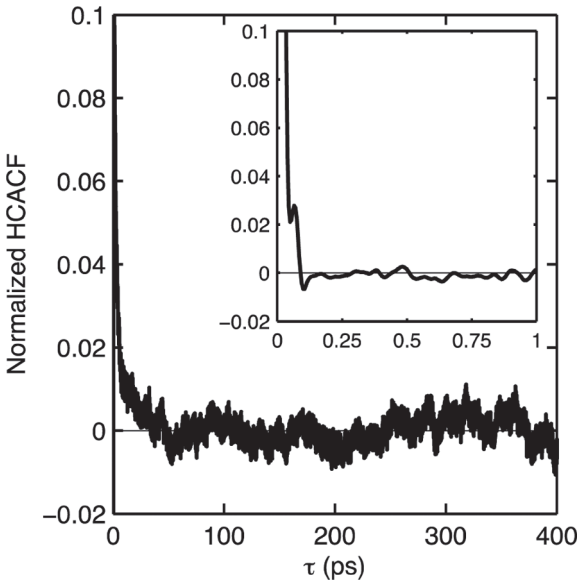

FIGURE 1
A representative plot of the normalized HCACF against correlation time for solid silicon at 1600 K. A characteristic reduction to zero is seen by $\tau = 50$ ps. The HCACF then randomly fluctuates about zero. The inset shows data for liquid silicon at 1700 K (note the change in axes scale). For liquid silicon the HCACF reaches zero by 0.25 ps, followed by the fluctuations.

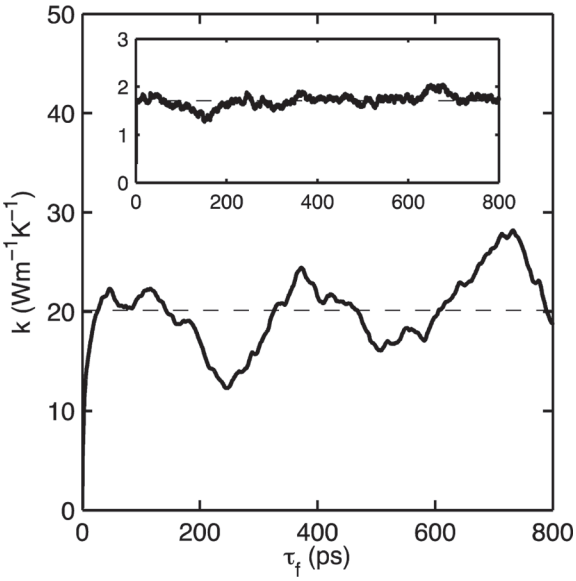

FIGURE 2
Conductivity versus integration limit in Eq. 1 for solid silicon at 1600 K derived from Figure 1. The wandering in the HCACF leads to ambiguity in the conductivity. The dashed line denotes the mean of the conductivity calculated over a range of integration times. Note that this plot depicts conductivity resulting from the HCACF of a single simulation. Inset: Conductivity of liquid silicon at 1700 K.

modes wrapping around the domain through the periodic boundaries (Lukes & Zhong, 2007; Volz & Chen, 2000). The result is that for longer correlation times, the integral in Eq. 1 does not converge to a definite value (Fig. 2). The oscillations of k extend to 800 ps, the limit of correlation time studied here. The value of conductivity in each simulation was obtained by averaging over the range of the integration times from 100 ps to 800 ps (solid phase) and from 1 ps to 800 ps (liquid phase). The simulations were repeated 10 times for each temperature and the results were averaged to obtain the final values listed in Tab. 2. Application of the linear extrapolation procedure (Hu, Evans, & Keblinski, 2011; Schelling, Phillpot, & Keblinski, 2002; Sellan, Landry, Turney, McGaughey, & Amon, 2010) to the results of the NEMD simulations produces conductivity values of 19.03 $Wm^{-1}K^{-1}$ at 1600 K and 1.85 $Wm^{-1}K^{-1}$ at 1700 K (Fig. 3), which agree with those obtained using EMD.

From the EMD and NEMD results discussed above, it is possible to draw comparison to experimental results for silicon near the melting temperature.

TABLE 2
Thermal conductivity predicted for Stillinger-Weber silicon in EMD simulations along with available experimental values (Yamasue, Susa, Fukuyama, & Nagata, 2002). The systems from 1400 K to 1600 K are in the solid state and the ones from 1700 K to 2000 K are in the liquid state. The uncertainty is equal to twice the standard deviation as derived from the individual sample variances (Burr, 1974)

T (K)	k, EMD ($Wm^{-1}K^{-1}$)	k, expt. ($Wm^{-1}K^{-1}$)
1400	28.42 ± 2.89	22.3 ± 2.4
1500	20.11 ± 2.93	20.1 ± 1.6
1600	19.71 ± 2.26	20.4 ± 1.0
1700	1.56 ± 0.21	56.5 ± 1.0
1800	1.61 ± 0.21	
1900	1.76 ± 0.26	
2000	1.78 ± 0.22	

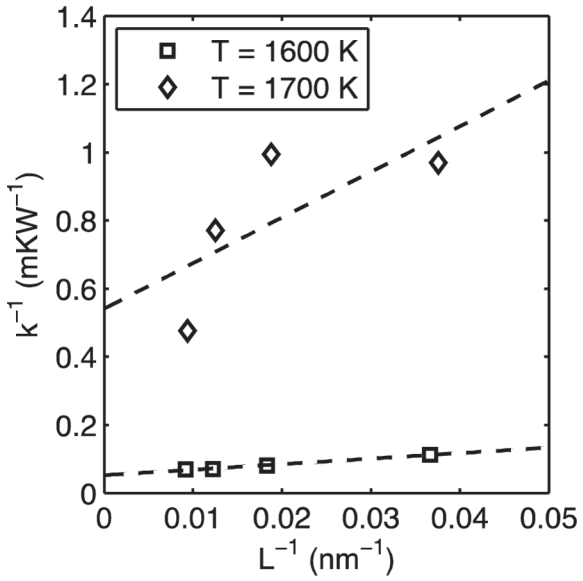

FIGURE 3
Inverse conductivity versus inverse length of solid and liquid phase silicon predicted in NEMD simulations. Extrapolation of the linear fit to $L^{-1} = 0$ returns an estimate of the bulk conductivity. The inverted ordinate creates the illusion of greater variability in the liquid system data compared to that of the solid system.

Experiments have found that silicon thermal conductivity ranges from 22.3 $Wm^{-1}K^{-1}$ to 20.4 $Wm^{-1}K^{-1}$ for temperatures from 1400 to 1600 K and is 56.5 $Wm^{-1}K^{-1}$ for liquid silicon at 1700 K (Yamasue, Susa, Fukuyama, & Nagata, 2002). The much larger value in the melted state is consistent with the onset of the electron dominated thermal transport. The EMD results for the solid phase are of the same order of magnitude, ranging from 28.42 to 19.71 $Wm^{-1}K^{-1}$. The fact that the Stillinger-Weber potential was fit to experimental data close to, and above, the melting point explains in part the similarity between the experimental and simulated conductivity values. The diffusion of electron-hole pairs is known to account for approximately 30–40% of the thermal conductivity of solid silicon close to the melting point, (Fulkerson, Moore, Williams, Graves, & McElroy, 1968; Glassbrenner & Slack, 1964). This indicates that the Stillinger-Weber potential substantially overestimates the phononic thermal conductivity in the solid phase compared to the actual silicon. Incidentally, this overestimation compensates for the inability of the classical MD to account for the electron-hole pair diffusion and allows one to accurately reproduce the high temperature thermal conductivity in MD simulations performed with the Stillinger-Weber potential.

In the liquid phase, the vibrational contribution found in the EMD simulations drops precipitously to 1.56 $Wm^{-1}K^{-1}$ at 1700 K, much smaller than the value of 56.5 $Wm^{-1}K^{-1}$ measured for real liquid silicon (Yamasue, Susa, Fukuyama, & Nagata, 2002), where the electronic contribution is dominant. In order to evaluate whether the Stillinger-Weber potential accurately reproduces the phononic thermal conductivity of the liquid phase silicon, we perform an analysis based on the Cahill-Pohl model developed for an amorphous solid (Cahill, Watson, & Pohl, 1992; Kaviany, 2008). According to this model, the phononic thermal conductivity can be estimated as

$$k = \left(\frac{\pi}{6}\right)^{\frac{1}{3}} k_B n^{\frac{2}{3}} \sum_m u_m \left(\frac{T}{T_{D,m}}\right)^2 \int_0^{\frac{T_{D,m}}{T}} \frac{x^3 e^x}{(e^x - 1)^2}\, dx \qquad (5)$$

where n is the material number density, m denotes an acoustic branch, u is the zone center group velocity, $T_{D,m}$ is the branch specific Debye temperature of $u_m \frac{\hbar}{k_B}(6\pi^2 n)^{\frac{1}{3}}$, and x is the reduced phonon energy: $\frac{\hbar\omega}{k_B T}$. The zone center acoustic velocity for each branch was determined using harmonic lattice dynamics with the appropriate number density (Gale & Rohl, 2003). The Cahill-Pohl model assumes that phonons have a mean free path equal to one half of their wavelength,

which fits amorphous solids well (Kaviany, 2008). The treatment of the liquid as an amorphous solid is in part justified by the small size of the simulated systems, which effectively prevents the convective heat transfer, leaving only conduction. The application of the Cahill-Pohl model results in a conductivity of about $1.39\,\mathrm{Wm^{-1}K^{-1}}$ for the liquid state, only slightly less than the values predicted in the simulations. This result confirms the mechanism behind the drastic reduction in thermal conductivity between the solid and liquid phases, i.e. the phase transition is accompanied by a sharp increase in the phonon scattering in the liquid structure. The quantitative agreement between the approximate Cahill-Pohl model and the predictions of molecular dynamics simulations suggest that the Stillinger-Weber potential provides an adequate description of the vibrational heat transfer in the liquid state. To ensure a realistic representation of the total thermal conductivity in liquid silicon, an electronic contribution of about $54.9\,\mathrm{Wm^{-1}K^{-1}}$ should be included into the model, e.g., by combining the molecular dynamics method with the continuum treatment of the electronic thermal conductivity within the two-temperature model (Ivanov & Zhigilei, 2003) or adding a specially designed thermostating procedure (Schall, Padgett, & Brenner, 2005).

CONCLUSIONS

In conclusion, EMD and NEMD simulations were employed to evaluate the phononic contribution to the thermal conductivity of high temperature silicon represented by the Stillinger-Weber potential. The potential is found to adequately reproduce the experimental values of thermal conductivity of solid silicon at high temperatures despite neglecting the contribution of the electron-hole pair diffusion. The simulated conductivity of the liquid phase also agreed with the theoretical phononic conductivity of the liquid phase, leading to an estimated electron conductivity of $54.9\,\mathrm{Wm^{-1}K^{-1}}$, to be included through a combined atomistic-continuum approach.

ACKNOWLEDGMENTS

Portions of this work were originally published by ASME in *Proceedings of the ASME 2011 International Mechanical Engineering Congress & Exposition* (Baker, Wu, Salaway, Zhigilei, & Norris, 2011). The authors would like to acknowledge the financial support of the Air Force Office of Scientific Research (Grant No. FA9550-09-1-0245) and the National Science Foundation (Grants No. CBET-1033919 and DMR-0907247). C.H.B. would like to thank J. C. Duda and T. S. English for helpful discussions on MD.

NOMENCLATURE

Symbols:

ε	atom energy [J]
$\vec{F}$	force [N]
$\hbar$	reduced Planck constant [Js]
k	thermal conductivity [$\mathrm{Wm^{-1}K^{-1}}$]
k_B	Boltzmann constant [$\mathrm{JK^{-1}}$]
L	length of non-equilibrium domain [m]
n	number density [$\mathrm{m^{-3}}$]
$\vec{q}$	heat flux [$\mathrm{Wm^{-2}}$]
$\vec{r}$	displacement [m]
$\vec{S}$	heat current [Wm]
t	time [s]
τ	correlation time [s]
T	temperature [K]
u	zone-center group velocity [$\mathrm{ms^{-1}}$]
v	atom velocity [$\mathrm{ms^{-1}}$]
V	volume [$\mathrm{m^3}$]
ω	phonon angular frequency [$\mathrm{s^{-1}}$]

Subscripts:

i, j, k	atom indices
m	phonon branch
μ, ν	vector components
t_f	time limit of data to be autocorrelated [s]
τ_f	correlation integral limit [s]
T_D	Debye temperature [K]

Acronyms:

EMD	equilibrium molecular dynamics
HCACF	heat current autocorrelation function

MD	molecular dynamics
NEMD	non-equilibrium molecular dynamics
TTM	two temperature model

WORKS CITED

1. Baker, C. H., Wu, C., Salaway, R. N., Zhigilei, L. V., & Norris, P. M. (2011). Vibrational contribution to thermal conductivity of silicon near solid-liquid transition. *Proceedings of the ASME*, IMECE 2011–64064.
2. Bass, M. (1983). *Laser Materials Processing* (1 ed., vol. 3). (M. Bass, Ed.) New York, New York: North-Holland.
3. Broughton, J. Q., & Li, X. P. (1987). Phase diagram of silicon by molecular dynamics. *Physical Review B, 35*, 9120.
4. Burr, I. W. (1974). *Applied Statistical Methods.* New York: Academic Press.
5. Cahill, D. G., Watson, S. K., & Pohl, R. O. (1992). Lower limit to the thermal conductivity of disordered crystals. *Physical Review B, 46*, 6131.
6. Duffy, D. M., & Rutherford, A. M. (2007). Including the effects of electronic stopping and electron-ion interactions in radiation damage simulations. *Journal of Physics: Condensed Matter, 19*, 016207.
7. Fulkerson, W., Moore, J. P., Williams, R. K., Graves, R. S., & McElroy, D. L. (1968). Thermal conductivity, electrical resistivity, and Seebeck coefficient of silicon from 100 to 1300 K. *Physical Review, 167*, 765.
8. Gale, J. D., & Rohl, A. L. (2003). The general utility lattice program (GULP). *Molecular Simulation, 29*, 291.
9. Glassbrenner, C. J., & Slack, G. A. (1964). Thermal conductivity of silicon and germanium from 3 K to the melting point. *Physical Review, 134*, A1058.
10. Head-Gordon, M., & Tully, J. C. (1995). Molecular dynamics with electronic frictions. *Journal of Chemical Physics, 103*, 10137.
11. Hoover, W. G. (1985). Canonical dynamics: equilibrium phase-space distributions. *Physical Review A, 31*, 1695.
12. Hu, L., Evans, W. J., & Keblinski, P. (2011). One-dimensional phonon effects in direct molecular dynamics method for thermal conductivity determination. *Journal of Applied Physics, 110*, 113511.
13. Ivanov, D. S., & Zhigilei, L. V. (2003). Combined atomistic-continuum modeling of short-pulse laser melting and disentigration of metal films. *Physical Review B, 68*, 064114.
14. Kaviany, M. (2008). *Heat Transfer Physics.* New York: Cambridge University Press.
15. Lee, Y., Biswas, R., Soukoulis, C. M., Wang, C. Z., Chan, C. T., & Ho, K. M. (1991). Molecular-dynamics simulation of thermal conductivity in amorphous silicon. *Physical Review B, 43*, 6573.
16. Lukes, J. R., & Zhong, H. (2007). Thermal conductivity of individual single-wall carbon nanotubes. *Journal of Heat Transfer, 129*, 705.
17. McQuarrie, D. A. (2000). *Statistical Mechanics.* Sausalito, California: University Science Books.
18. Migliore, L. (1996). *Laser Materials Processing* (1 ed.). (L. Migliore, Ed.) New York: Marcel Dekker, Inc.
19. Miller, J. C., & Haglund, R. F (1998). *Laser Ablation and Desorption* (1 ed., Vol. 30). (J. C. Miller, & R. F. Haglund, Eds.) New York: Academic Press, Inc.
20. Nosé, S. (1984). A unified formulation of the constant temperature molecular dynamics methods. *Journal of Chemical Physics, 81*, 511.
21. Ohsaka, K., Chung, S. K., Rhim, W. K., & Holzer, J. C. (1997). Densities of Si determined by an image digitizing technique in combination with an electrostatic levitator. *Applied Physics Letters, 70*, 423.
22. Phillips, C. L., Magyar, R. J., & Crozier, P. S. (2010). A two-temperature model of radiation damage in α-quartz. *Journal of Chemical Physics, 133*, 144711.
23. Plimpton, S. (1995). Fast parallel algorithms for short-range molecular dynamics. *Journal of Computational Physics, 117*, 1.
24. Poate, J. M., & Mayer, J. W. (1982). *Laser Annealing of Semiconductors* (1 ed.). (J. W. J. M. Poate, Ed.) New York: Academic Press, Inc.
25. Rutherford, A. M., & Duffy, D. M. (2007). The effect of electron-ion interactions on radiation damage simulations. *Journal of Physics: Condensed Matter, 19*, 496201.
26. Salaway, R. N., Hopkins, P. E., Norris, P. M., & Stevens, R. J. (2008). Phonon contribution to thermal boundary conductance at metal interfaces using embedded atom method simulations. *International Journal of Thermophysics, 29*, 1987.
27. Schall, J. D., Padgett, C. W., & Brenner, D. W. (2005). Ad hoc continuum-atomistic thermostat for modeling heat flow in molecular dynamics simulations. *Molecular Simulation, 31*, 283.
28. Schelling, P. K., Phillpot, S. R., & Keblinski, P. (2002). Comparison of atomic-level simulation methods for computing thermal conductivity. *Physical Review B, 65*, 144306.
29. Sellan, D. P., Landry, E. S., Turney, J. E., McGaughey, A. J., & Amon, C. H. (2010). Size effects in the molecular dynamics thermal conductivity predictions. *Physical Review B, 81*, 214305.
30. Stich, I., Car, R., & Parrinello, M. (1991). Structural, bonding, dynamical, and electronic properties of liquid silicon: an ab initio molecular-dynamics study. *Physical Review B, 44*, 4262.
31. Stillinger, F. H., & Weber, T. A. (1985). Computer simulation of local order in condensed phases of silicon. *Physical Review B, 31*, 5262.
32. Stillinger, F. H., & Weber, T. A. (1986). Erratum: computer simulation of local order in condensed phases of silicon. *Physical Review B, 33*, 1451.
33. Volz, S. G., & Chen, G. (2000). Molecular-dynamics simulation of thermal conductivity of silicon crystals. *Physical Review B, 61*, 2651.
34. Yamasue, E., Susa, M., Fukuyama, H., & Nagata, K. (2002). Thermal conductivities of silicon and germanium in solid and liquid states measured by non-stationary hot wire method with silica coated probe. *Journal of Crystal Growth, 234*, 121.